TECHNICAL PAPER

JOURNAL OF THE SOUTH AFRICAN INSTITUTION OF CIVIL ENGINEERING
ISSN 1021-2019 (print) | ISSN 2309-8775 (online)
Vol 66 No 3, September 2024, Pages 14–28, Paper 1487

PIERRE CLOETE (PrTechEng, MSAICE) obtained an MEng in Civil Engineering from Stellenbosch University and a BSc (Hons) in Civil Engineering (Water Resources) from the University of Pretoria. He currently works in Zutari's Pretoria office as a hydraulic designer. His research interests include hydraulic modelling, and open channel and dam spillway hydraulics.

Contact details:
Zutari
Riverwalk Office Park
41 Matroosberg Road
Ashley Gardens Extension 6
Pretoria 0081
South Africa
E: pierrecloete@yahoo.com

DR ADÈLE BOSMAN (PrEng), who is a Senior Lecturer in the Department of Civil Engineering at Stellenbosch University, has more than 15 years of experience in the water industry. She specialises in river hydraulics, dam engineering and sedimentation, with a particular focus on the design of hydraulic structures and rock scour. She holds an MSc in Civil Engineering and a PhD in hydraulics and rock mechanics, both from Stellenbosch University. Her expertise includes addressing scour and erosion problems downstream of dams and appurtenant structures. Before joining Stellenbosch University in 2013, she worked for consulting engineers in South Africa for four years.

Contact details:
Civil Engineering Department
Water Division
Stellenbosch University
Private Bag X1
Matieland 7602
South Africa
E: abosman2@sun.ac.za

Stepped chute energy dissipation structure downstream of a low-level river crossing for embankment protection

P Cloete, A Bosman

A low-level river crossing is an economic means of providing access for lower-order roads during high-frequency flood events. Conventionally, culverts are employed to enable the flow to traverse the road, albeit with allowance for overtopping. This overtopping flow from the approach roads, however, possesses the potential to cause erosion of the downstream embankment, thereby jeopardising the foundational integrity of the structure. A physical modelling study was undertaken to investigate the hydraulic performance of stepped chutes in terms of flow patterns, air-water flow properties, and energy dissipation. Various types of stepped chutes were investigated, namely horizontal steps with a chute wall, horizontal steps without a chute wall but with riprap placed directly downstream of each chute, step-inclined steps (backward sloping), steps with pooled cascades, and steps with baffle blocks. Notably, chutes with horizontal steps were the most efficient configuration in terms of relative energy dissipation. Furthermore, this research culminated in the formulation of a new regression formula to establish a quantifiable relationship between the required step length and the overflow depth and discharge, thereby offering a valuable tool for design purposes.

Keywords: low-level river crossing, stepped chute, nappe flow, energy dissipation, erosion protection, physical modelling

INTRODUCTION

A low-level river crossing (LLRC) is a structure that facilitates the crossing of either a river or stream for lower-order roads. These crossings are economically advantageous because they allow for overtopping flow (Pienaar & Kruger 2013), making them a preferred option for community access.

A low-level river crossing is typically classified as either a drift or a causeway, often referred to as a vented causeway (Johannessen 2008). A drift represents a river crossing where water flow can solely traverse the travelled road surface, whereas a causeway incorporates culvert openings underneath, allowing water to pass through. Typically, a low-level river crossing consists of a main deck, approach roads and multiple openings underneath the deck as illustrated in Figure 1. The height from the riverbed to the deck is normally less than 2 m (Pienaar & Kruger 2013).

During high river flow events, which then overtop the low-level river crossing, the flow traversing the approach roads tends to accelerate, discharging onto and eroding the downstream abutting embankments as illustrated in Figure 2.

The erosion of the downstream embankments is typically protected by placing a revetment constructed from riprap. Nonetheless, the construction of such a protection system may prove to be expensive if an adequate source of suitable rock is not readily available nearby. A possible mitigation measure investigated in this study is the construction of a stepped chute downstream of the approach roads. This chute comprises a series of vertical drops (steps) designed to efficiently dissipate excess energy.

This study aimed to investigate the hydrodynamics and energy dissipation characteristics of a stepped chute situated downstream of a low-level road crossing,

Cloete P, Bosman A. Stepped chute energy dissipation structure downstream of a low-level river crossing for embankment protection. J. S. Afr. Inst. Civ. Eng. 2024:66(3), Art. #1487, 15 pages. http://dx.doi.org/10.17159/2309-8775/2024/v66n3a2

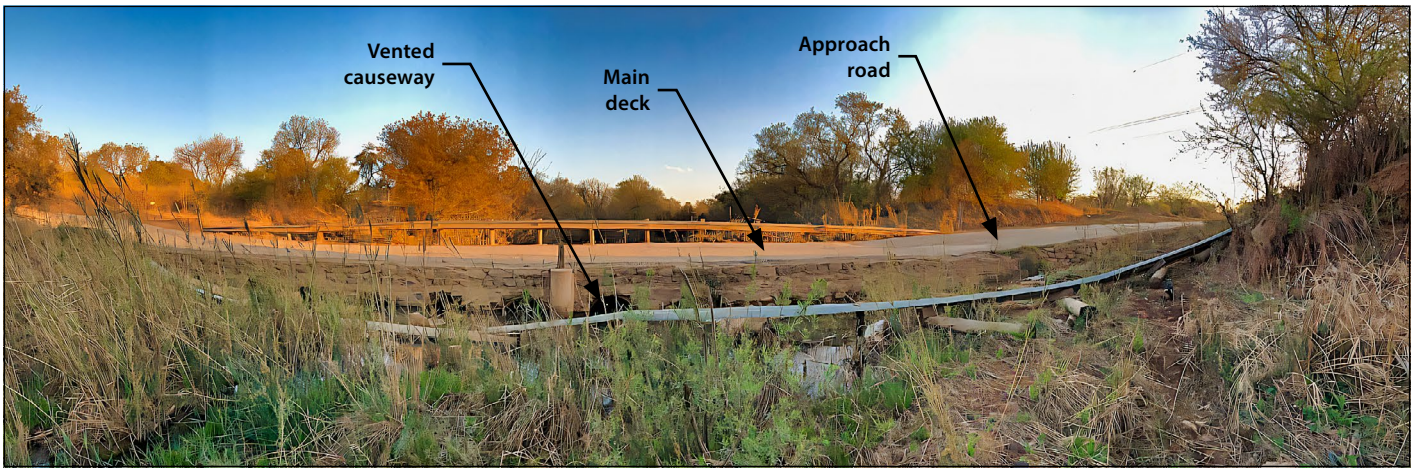

Figure 1 Photograph downstream of a low-level river crossing (R223 crossing the Pienaars River, Pretoria, South Africa)

employing a physical model. The flow patterns and energy dissipation were investigated for different step types, namely horizontal steps with an end chute sidewall, horizontal steps without a sidewall but with riprap directly downstream of each chute step, inclined steps (backward sloping), steps with pooled cascades, and steps with baffle blocks. These step types were experimentally investigated with 55 physical model tests for a range of flow rates and overflow depths. A non-dimensional formula for determining the length of the step required was developed based on the experimental test results and using multi-linear regression analysis.

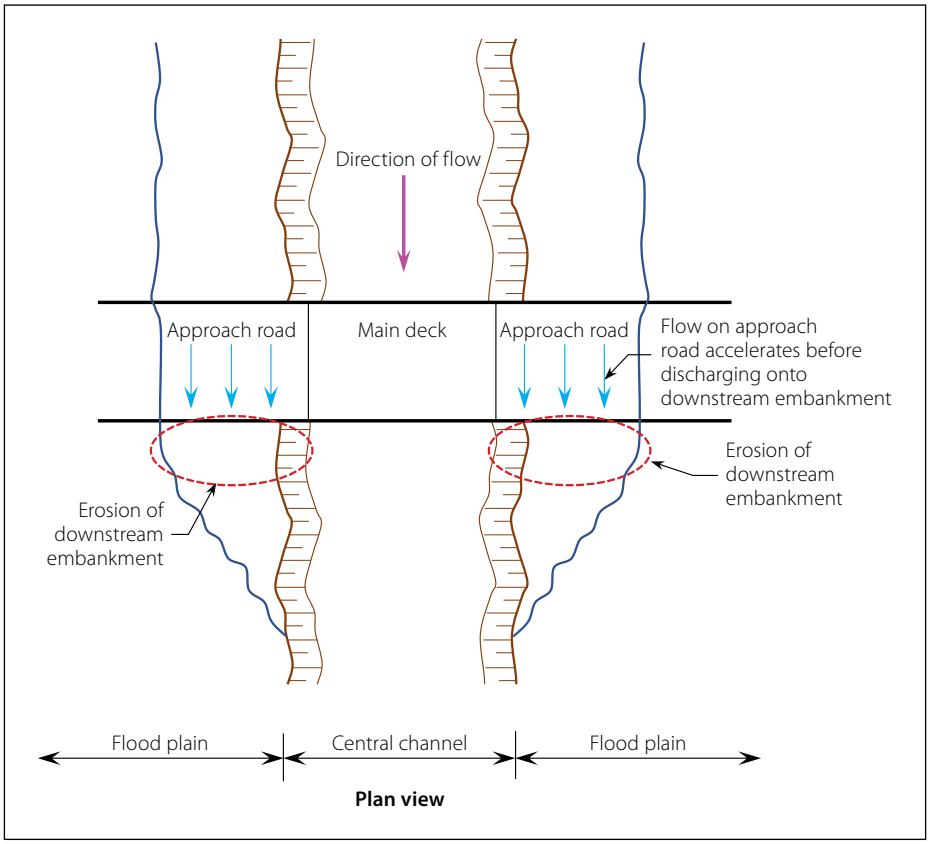

Figure 2 Plan view of low-level river crossing

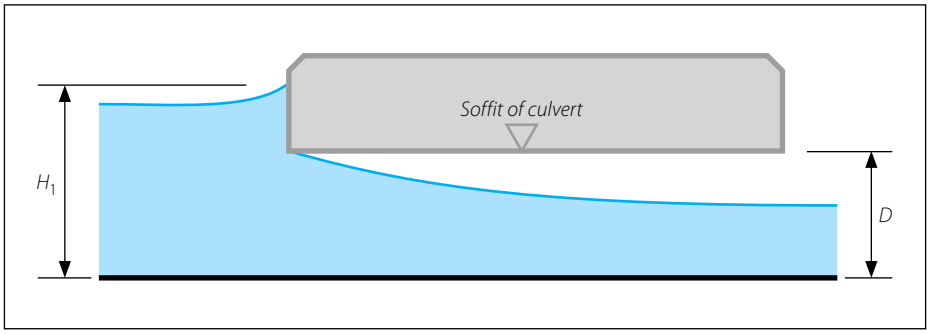

Figure 3 Flow through a culvert under inlet control

LOW-LEVEL RIVER CROSSING AND STEPPED CHUTE FLOW PROPERTIES

Flow through culverts

The hydraulic design of a causeway mirrors that of lesser culverts (where flow passes through the open conduits) and normally adheres to either upstream (inlet) control or downstream (outlet) control flow conditions. Inlet control occurs when critical flow conditions occur at the inlet of the culvert, indicating that the entrance flow capacity is less than the barrel. The water surface does not make contact with the culvert's soffit inside the barrel for a damming height to culvert height ratio (H/D) of less than 1.2. However, when the H/D ratio exceeds 1.2, the water surface does come into contact with the soffit at the inlet, effectively acting as a sluice gate (Henderson 1966). Figure 3 illustrates flow through a culvert during inlet control.

Equations 1 and 2 can be used to calculate the discharge for either a square or rectangular culvert under inlet control (Rooseboom & Van Vuuren 2013):

For: $0 < \frac{H_1}{D} < 1.2$

$$Q = \frac{2}{3} C_b \, w_{culvert} \, H_1 \sqrt{\frac{2}{3} g H_1} \qquad (1)$$

For: $\frac{H_1}{D} > 1.2$

$$Q = C_h \, w_{culvert} \, D \sqrt{2g(H_1 - C_h D)} \qquad (2)$$

Where:

Q is the discharge through the culvert (m^3/s)

C_b is the dimensionless coefficient expressing the effect of width contraction in the flow (C_b = 0.9 for square inlets and C_b = 1.0 for rounded inlets where $r > 0.1w_{culvert}$)

r is the radius of the rounding at the inlet in metres

C_h is the dimensionless coefficient of contraction in the vertical plane (C_h = 0.6 for square inlets and C_h = 0.8 for rounded inlets)

$w_{culvert}$ is the width of the culvert opening (m)

D is the height of the culvert opening (m)

H_1 is the upstream energy head of the culvert (m) and g is the gravitational acceleration (9.81 m/s^2).

When the tailwater influences the upstream conditions of the low-level river crossing, outlet control will occur. Outlet control conditions were, however, not considered during this study.

Stepped chute spillways

Increased interest has been shown in stepped spillways due to the advantages in the construction of roller-compacted concrete (RCC) dams, as well as the considerable amount of energy dissipation that leads to reduced stilling basin sizes (Khatsuria 2005). Flow down a stepped chute typically exhibits three distinct flow regimes, namely nappe flow, transition flow and skimming flow. The step geometry (step height h and length l) can be manipulated to dictate the flow regime, as illustrated in Figure 4.

The nappe flow regime is characterised by flow-free falling as a jet from one step, which then impinges on the next step. Immediately after impingement, the flow is supercritical and, if the step is long enough, can lead to either a fully developed or partially developed hydraulic jump (sub-regimes NA1 and NA2 respectively), as illustrated in Figure 5.

The nappe geometry for horizontal steps can be defined using Equations 3 to 7 (where all dimensions are in metres) and is illustrated in Figure 5 if the nappe is ventilated (Chanson 2001):

$$y_b = 0.715y_c \quad (3)$$

$$y_1 = 0.54h\left[\frac{y_c}{h}\right]^{1.275} \quad (4)$$

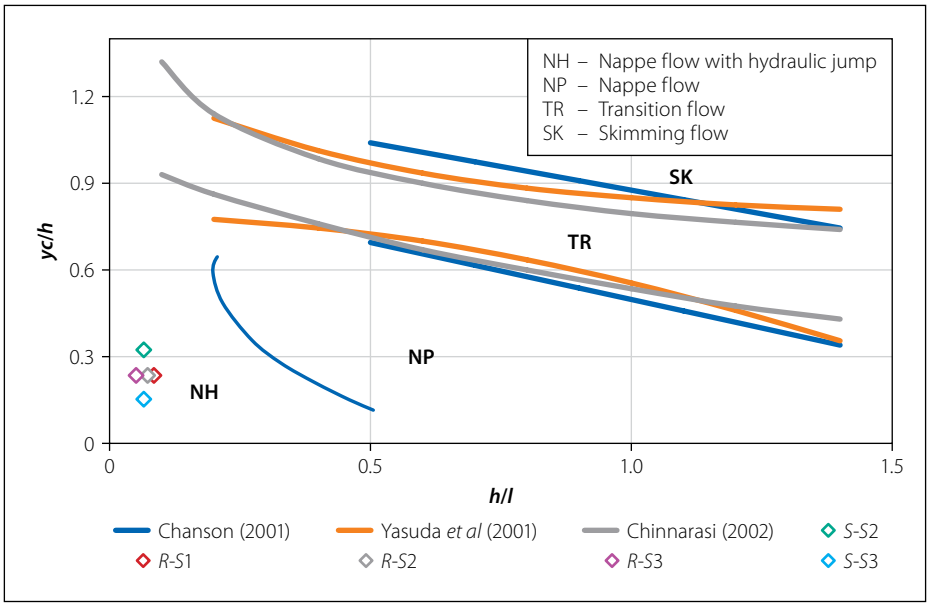

Figure 4 Flow regimes on stepped spillways (adapted from Khatsuria 2005)

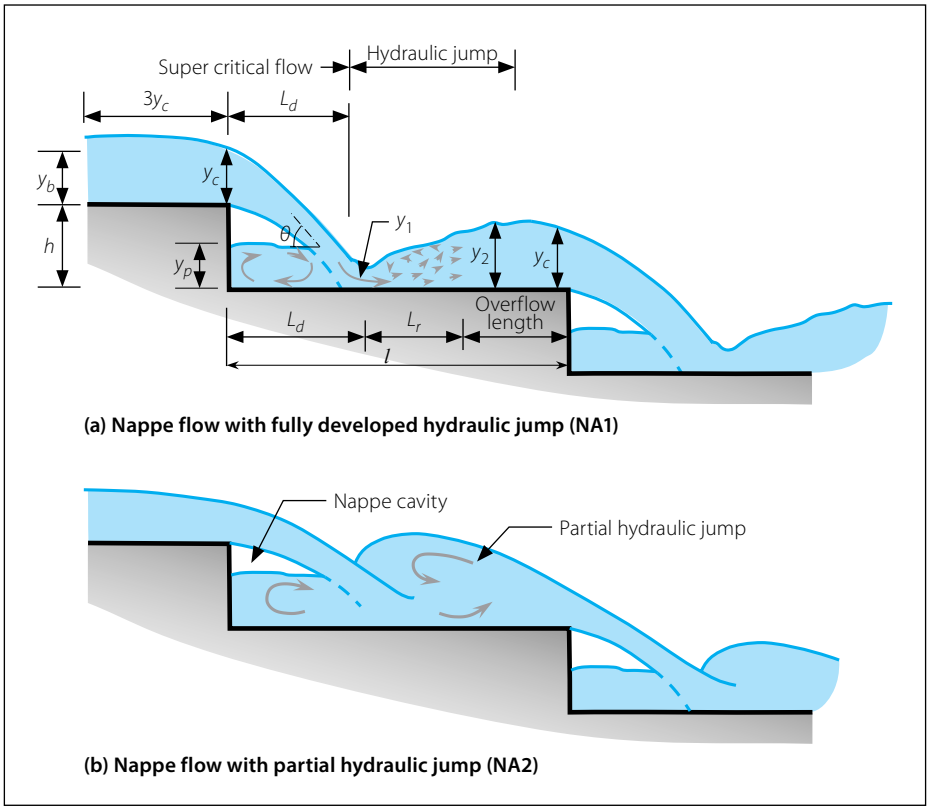

(a) Nappe flow with fully developed hydraulic jump (NA1)

(b) Nappe flow with partial hydraulic jump (NA2)

Figure 5 Nappe flow with (a) fully and (b) partially developed hydraulic jump

$$y_2 = 1.66h\left[\frac{y_c}{h}\right]^{0.81} \quad (5)$$

$$y_p = h\left[\frac{y_c}{h}\right]^{0.66} \quad (6)$$

$$L_d = 4.3h\left[\frac{y_c}{h}\right]^{0.81} \quad (7)$$

The length of the roller (L_r), measured in metres, can be calculated using Equation 8 (Hager *et al* 1990):

$$L_r = 8y_1(Fr_1 - 1.5) \quad (8)$$

Where:

Fr_1 is the dimensionless Froude number

y_1 is the flow depth (m) directly upstream of the hydraulic jump.

According to Peyras *et al* (1992), Equations 3 to 8 can also be applied, with reasonable accuracy, to nappe flows with partially developed hydraulic jumps.

Ventilation of the nappe

In scenarios where an uncontracted nappe is closed on both sides, artificial ventilation of the nappe may be required, as the falling

nappe draws air from the cavity between the nappe and the pool located behind the nappe. The entrained air is subsequently transported downstream, leading to sub-atmospheric pressure within the cavity behind the nappe (Chanson 2001). Bos (1989) developed a formula (Equation 9) for the maximum air demand required for full aeration of a nappe which had no restriction on the approach flow Froude number:

$$Q_{air} = 0.1\frac{Q_w}{\left[\frac{y_p}{y_{top}}\right]^{1.5}} \quad (9)$$

Where:

Q_{air} is the nappe aeration (m^3/s)

Q_w is the discharge of the nappe (m^3/s)

y_p is the pool depth beneath the nappe in metres

y_{top} is the flow depth on the top step (m).

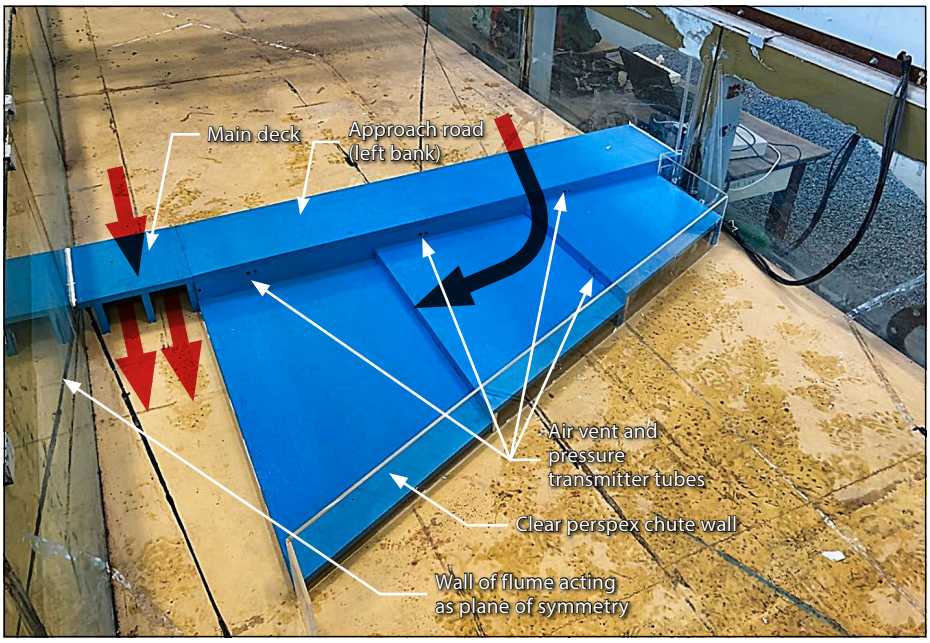

Figure 6 Scaled model of low-level river crossing with horizontal stepped chute, viewed from the downstream perspective looking upstream

EXPERIMENTAL SETUP

Model layout

The hydraulic performance of stepped chutes downstream of a low-level river crossing was investigated by means of a physical model. An arbitrary, though typical, prototype low-level river crossing with stepped chute at a scale of 1:15 was selected. The symmetrical and geometric nature of a typical low-level river crossing allowed for a significant reduction in the size of the model, yet still allowed the flow field over the road and chute to be represented in its entirety.

The model comprised half of the main road deck with two-and-a-half (2.5) culverts underneath, together with the approach road as shown in Figure 6. This symmetrical configuration ensured representative

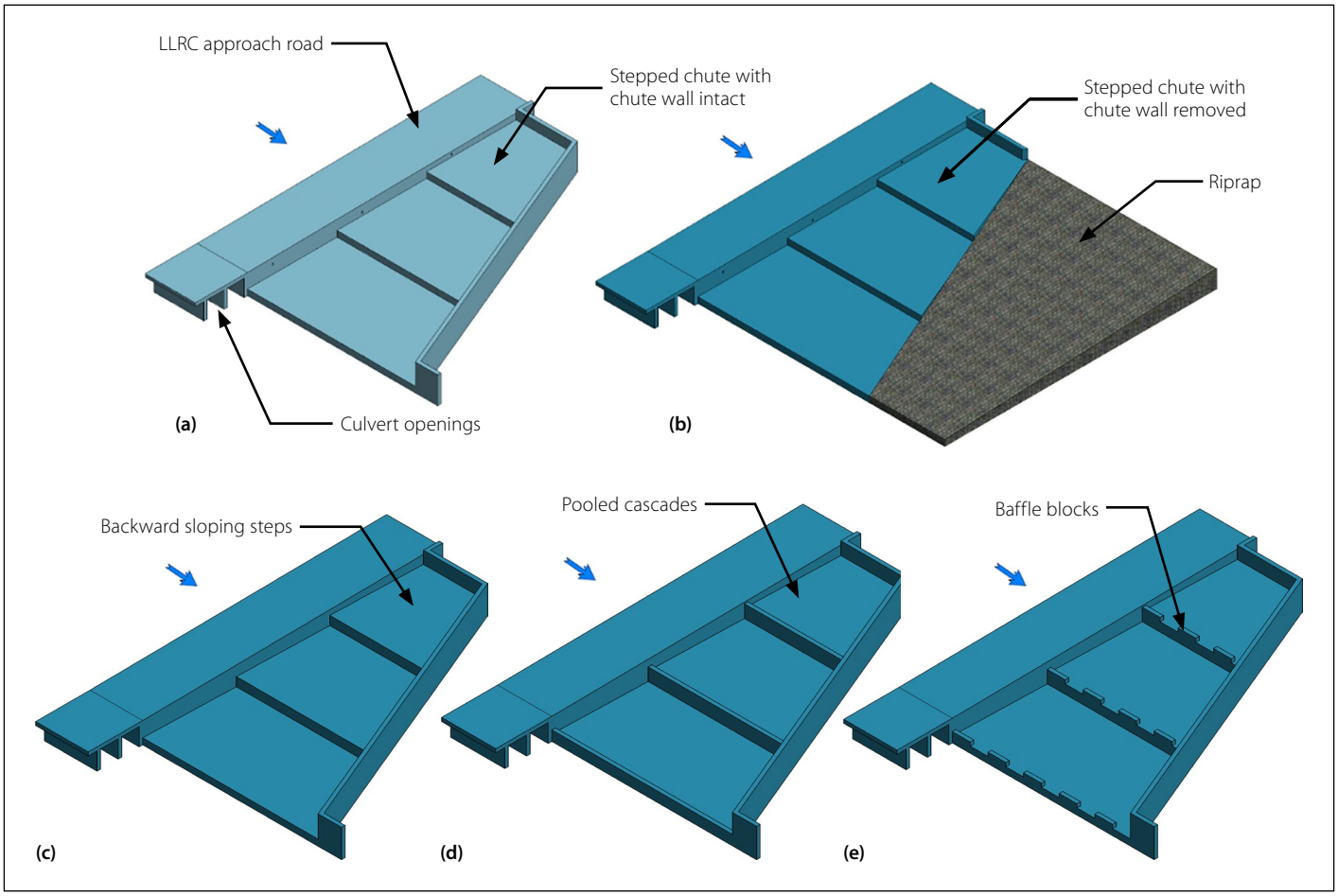

Figure 7 Model setup variations: (a) chute wall intact, (b) chute wall removed and riprap added, (c) backward sloping steps, (d) steps with pooled cascades, (e) steps with baffle blocks

interaction between culvert flow and chute flow. The model was installed in a 2 m wide flume with adjustable longitudinal slope. The longitudinal slope was set to 0% to ensure that the hydraulic model functioned as a control, and that upstream (sub-critical flow) conditions would not have an effect on the model operation.

The five model configurations tested to investigate the hydraulic performance of the stepped chute were horizontal steps with an end chute sidewall, horizontal steps with riprap directly downstream of each chute step, backward sloping steps, steps with pooled cascades, and steps with baffle blocks as illustrated in Figure 7 (page 17). A combination of the five model configurations was tested with the culverts (one or more) open and with the culverts closed to observe the effect on the flow patterns if the road is inundated. Riprap was also integrated into the model setup, as illustrated in Figure 7(b), to observe the change in flow patterns on the chute. It is worth noting that, while the riprap was sized to be stable under the test flow conditions, the primary focus was not to determine the required stable riprap size to be used in combination with the stepped chute.

The 1:15 model scale was selected to not only limit scaling effects, but also to allow for practical limitation on the various measurements. The chosen scale, together with adherence to the minimum overflow depth, limits surface tension effects to ensure that the water-air interface of the overflow nappe and air entrainment on the chute steps did not have an inordinately large effect on the behaviour of the flow. The dominant forces applicable to the model study were inertia and gravity, as free surface flow conditions prevailed. The model was therefore designed using Froude similitude (Vos 2011). The Reynolds and Weber numbers were sufficiently large to minimise scale effects.

The walls of the approach road and chute steps of the model were fitted with small-diameter pipes to allow for the remote measurement of the air pressure and velocities of the nappe ventilation using high-frequency pressure transmitters and a Lutron hot-wire anemometer, respectively. Additional data that was collected included the discharge, water level, flow profiles, and visual observations. Measurement uncertainty of the various instruments was minimised by repeating tests, using high-frequency data capture, and using multiple sampling points. Water levels and flow profiles were measured with an accuracy of 1 mm. Discharges were measured using a DN100 Flowmetrix Magflow

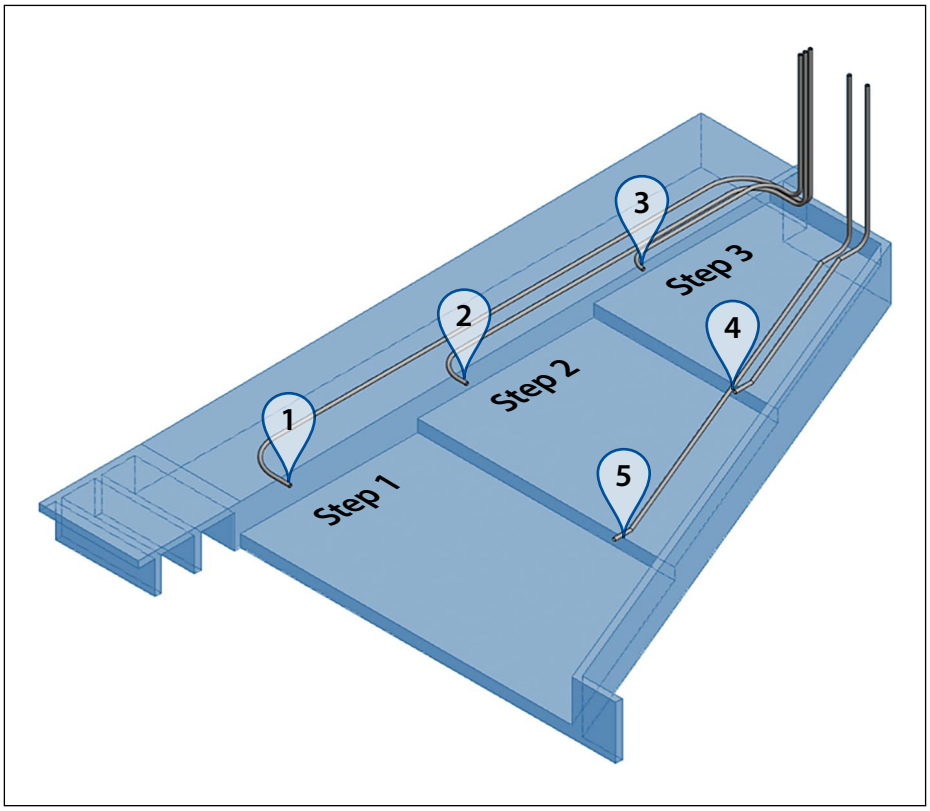

Figure 8 Nappe ventilation installation

flow meter with an accuracy of ±0.5%, as well as with a V-notch weir with a precision of 1 mm. The pressure fluctuations were measured with Wika S-10 pressure transmitters. The transmitter locations coincided with the nappe ventilation pipe positions indicated in Figure 8. The transmitters had a measuring range of ±100 mbar, a repeatability of ±0.1% and an accuracy of ±0.2%. The Lutron hot-wire anemometer used to measure airflow velocities in the nappe ventilation pipes had an accuracy of ±5% and a measuring range of 0.2 – 20 m/s. Equation 9 was used as an initial estimation of the nappe ventilation requirement of the prototype, as it had no limitation on the approach Froude number. Further details regarding the model construction, setup, data capturing methodologies, measurement accuracies, and scaling effects are described in Cloete (2019).

Model properties

The main components of the model, and the corresponding design recommendation and procedures that were used are summarised in Table 1.

Low-level river crossing

The design of the low-level river crossing consisted of the flow through the culverts and the flow over the low-level river crossing. The overflow depth at the crossing directly impacted both the flow rate over and through the low-level river crossing. Pienaar and Kruger (2013) recommend that the maximum allowable overflow depths for low-level river crossings are 100 mm for supercritical flow and 150 mm for sub-critical flow due to safety considerations.

However, there exists the possibility of the designed capacity of the low-level river

Table 1 Hydraulic model design recommendations and procedures

Model component	Design recommendations and/or procedures
Low-level river crossing overflow	■ For 0% cross fall: assume critical flow over the river crossing. ■ For >0% cross fall in the downstream direction: use either Manning or Chezy's equation for open channel flow.
Approach road	Chapter 6, *SANRAL Road Drainage Manual*, 6th Edition's recommendations for low-level river crossing approach roads (Pienaar & Kruger 2013). The prototype approach road grade was 1.25%.
Culvert through low-level river crossing	Chapter 7, *SANRAL Road Drainage Manual*, 6th Edition's recommendations for inlet control (Rooseboom & Van Vuuren 2013).
Stepped chute	Chanson's (1994) Hydraulics of nappe flow regime above stepped chutes and spillways.

crossing being exceeded in certain circumstances. This is because low-level river crossings are normally designed to accommodate relatively low recurrence intervals, typically within the range of 1:2 to 1:10 year return periods, and because it is further recommended that the approach roads are extended above the 1:10 year flood level (Pienaar & Kruger 2013). This scenario where the capacity is exceeded could result in higher overflow depths and increased levels of damage to the crossing. To address this potential scenario, a maximum prototype design overflow depth of 300 mm (an equivalent model overflow depth of 20 mm) was therefore selected to make allowance for such events. The model, however, was tested in five equal depth increments starting from 60 mm (prototype depth) to the maximum overflow depth of 300 mm (model depth ranges from 4 mm to 20 mm).

To use the full width of the test channel, an approach road gradient of 1.25% was chosen. This gradient falls well within the recommended maximum approach road gradients for paved and unpaved roads, as outlined by Pienaar and Kruger (2013).

The prototype approach road was designed with a width of 4.5 m, which is typical for a single-lane road, and includes 0.25 m wide guide blocks on both sides. A level deck (0% cross-fall) was selected. The level deck effectively transformed the road into a hydraulic control, akin to a broad-crested weir, which resulted in critical flow conditions over the low-level river crossing. Additionally, it simplified the flow depth measurement on the deck, streamlining the data collection process.

The prototype low-level river crossing was designed to have five square culvert openings, each measuring 1.5 m × 1.5 m. However, the model was bisected along the plane of symmetry, resulting in only two and a half (2.5) culverts for the hydraulic model. Initial testing with 2.5 open culverts caused complete inundation of the bottom step (step 1 as indicated in Figure 8). As a result, the testing and data collection of the model were executed with only one culvert open to avoid excessive inundation of the stepped chute. The recorded test flow depths, along with the corresponding flow rates over half of the crossing, through one culvert opening, and for the entire model are listed in Table 2.

Table 2 Low-level river crossing overflow test depths with corresponding flow rates

Low-level river crossing overflow depths		Total flow over half of the crossing	Total flow through a single culvert opening	Total flow through model
60 mm (4 mm)	A	0.3 m³/s (0.3 L/s)	5.9 m³/s (6.8 L/s)	6.2 m³/s (7.1 L/s)
120 mm (8 mm)	B	1.0 m³/s (1.1 L/s)	6.2 m³/s (7.1 L/s)	7.2 m³/s (8.2 L/s)
180 mm (12 mm)	C	2.2 m³/s (2.6 L/s)	6.4 m³/s (7.3 L/s)	8.6 m³/s (9.9 L/s)
240 mm (16 mm)	D	4.1 m³/s (4.7 L/s)	6.6 m³/s (7.6 L/s)	10.7 m³/s (12.3 L/s)
300 mm (20 mm)	E	6.5 m³/s (7.5 L/s)	6.8 m³/s (7.8 L/s)	13.3 m³/s (15.3 L/s)

Note: Values indicated in parentheses refer to scaled hydraulic model values.

Stepped chute

For the design of the stepped chute, the flow dynamics were modelled with the concept of flow initially forming a nappe from the approach road and subsequently impinging on each of the chute steps. Beyond the nappe impingement point, the flow transitioned to a supercritical state, continuing until a hydraulic jump formed on the step. The same flow profile would occur from one chute step onto the next in the direction of the stepped chute.

To define the geometry of the chute, Equations 3 to 8 were used to establish the nappe geometry from the approach road onto each step. Flow directed towards the central region of the model encountered less resistance, resulting in higher approach velocities. Nevertheless, for the initial determination of the chute configuration, the flow onto each individual step was ascertained through proportional allocation, dividing the flow along the approach road into the flow area above each chute step. The instabilities observed in the model at the boundaries generally manifested in flow scenarios where the Reynolds and Weber numbers were sufficiently large to minimise any scale effects. The chosen scale limited the effect of surface tension to ensure that the air-water interface of the overflow nappe and the air entrainment in the downstream water body did not have an inordinately large effect on the behaviour observed in the model as suggested by the accepted guidelines and assumptions presented in Heller (2011). Consequently, the flow depth and step height used to calculate the nappe geometry for each step were selected at the point where the deepest flow depth (and flow concentration) was expected to occur. As an example, for the flow impinging on step 2, a vertical line was projected from the brink of step 2, and the step height was determined as the difference in elevation between the approach road surface and the top of step 2 (refer to dimension h_{R-S2} in Figure 9).

The same principles were applied for the calculation of the flow depth after nappe had impinged on each step, which was subsequently used to determine the length of the hydraulic jump roller and the conjugate flow depth. Figure 9 provides a visual representation of the positions of the nappe geometry variables, illustrating their interaction as the nappe formed from the approach road onto the stepped chute. Table 3 lists the calculated prototype nappe drop lengths ($L_{d\,R-S}$) and hydraulic jump roller lengths ($L_{r\,R-S}$) that resulted from the flow originating from the approach road to each individual step.

The flow along the stepped chute was accumulatively calculated, starting from the top step (step 3) to the bottom step (step 1). These cumulative discharges were used to determine the nappe geometry from one step

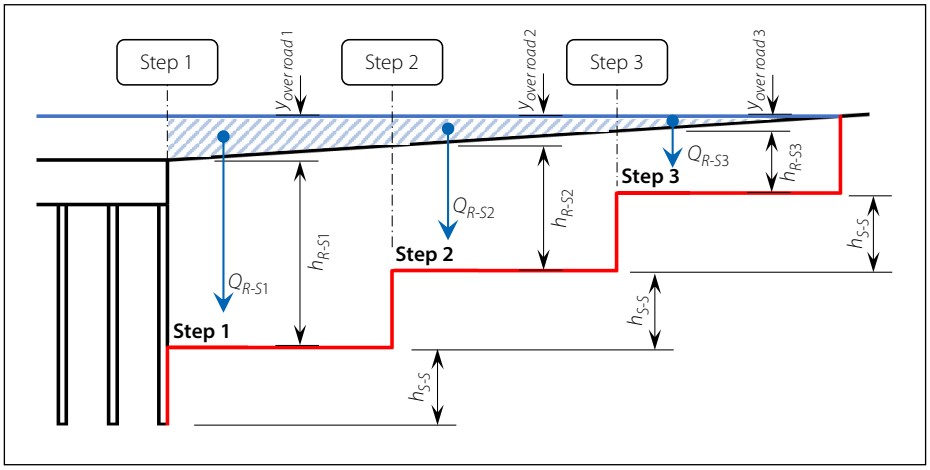

Figure 9 Downstream stepped chute profile indicating positions of overflow depths ($y_{over\ road}$) and nappe fall heights (h_{R-S})

Table 3 Nappe drop lengths and hydraulic jump roller lengths from the road to the steps

Prototype: flow from road to steps (m^3/s)	Prototype: nappe drop length ($L_{d\,R\text{-}S}$) (m)	Prototype: hydraulic jump roller length ($L_{r\,R\text{-}S}$) (m)	Prototype: total length ($L_{d\,R\text{-}S} + L_{r\,R\text{-}S}$) (m)	Model: total length ($L_{d\,R\text{-}S} + L_{r\,R\text{-}S}$) (mm)
$Q_{R\text{-}S3}$ = 0.52	0.57	0.44	1.01	67
$Q_{R\text{-}S2}$ = 1.50	1.13	0.99	2.12	141
$Q_{R\text{-}S1}$ = 2.62	1.70	1.23	2.93	195

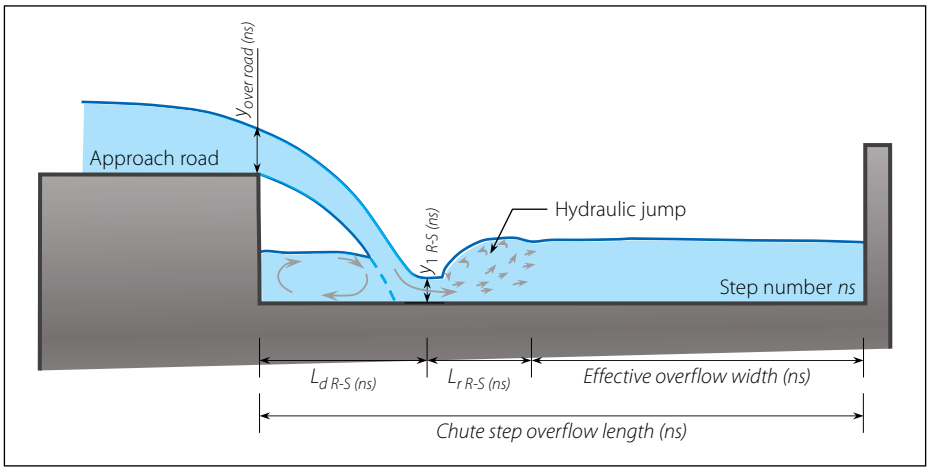

Figure 10 Cross-sectional view for determining stepped chute effective overflow length

Table 4 Nappe drop lengths and hydraulic jump roller lengths from one step to the next

Prototype: cumulative flow from step ($Q_{S\text{-}S\ (ns)}$) (m^3/s)	Prototype: nappe drop length ($L_{d\,S\text{-}S}$) (m)	Prototype: hydraulic jump roller length ($L_{r\,S\text{-}S}$) (m)	Prototype: total length ($L_{d\,S\text{-}S} + L_{r\,S\text{-}S}$) (m)	Model: total length ($L_{d\,S\text{-}S} + L_{r\,S\text{-}S}$) (mm)
$Q_{S\text{-}S3}$ = 0.523	0.50	0.69	1.18	79
$Q_{S\text{-}S2}$ = 2.092	0.91	0.96	1.87	124
$Q_{S\text{-}S1}$ = 4.708	1.24	1.10	2.34	156

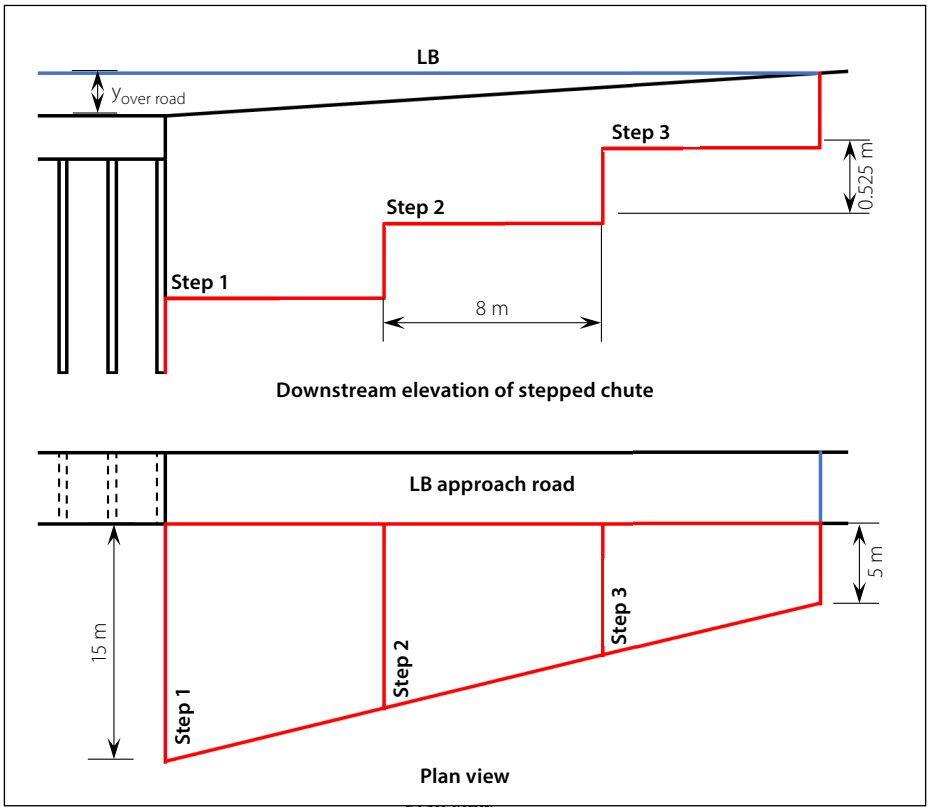

Figure 11 Prototype chute dimensions (not to scale)

to the next. The step height ($h_{S\text{–}S}$) remained constant (at a prototype value of 525 mm). The critical depth at the brink of each step was a function of the nappe geometry calculated for flow from the approach road onto each specific step. Furthermore, the effective overflow width at the brink of each step was assumed to exclude the nappe drop length and hydraulic jump length that resulted from the flow originating from the approach road onto the steps, as illustrated in Figure 10.

The stepped chute dimensions were determined through an iterative selection process, primarily driven by interplay between the nappe geometry falling from the approach road and its influence on the nappe geometry from one step to the next. This iterative process was guided by three conditions which needed to be adhered to when selecting the appropriate chute dimensions:

1. The *conjugate flow depth* on one step should not exceed the step height, as doing so could lead to inundation of the previous step, potentially altering the flow regime to either transition or skimming flow.
2. Chanson (1994) asserted that the combined length of the drop (L_d) and the length of the roller (L_r) should ideally be shorter than the total length of the step (l). This criterion ensures that a fully developed hydraulic jump occurs, leading to higher rates of energy dissipation. Therefore, it is advantageous to maintain step lengths that are sufficiently long enough for hydraulic jump formation, which promotes effective energy dissipation.
3. The nappe flow conditions must be maintained for flow from the road onto the steps, as well as flow from one step to the next (refer to Figure 4).

Table 4 provides a summary of the calculated nappe drop length ($L_{d\,S\text{–}S}$) and hydraulic jump roller lengths ($L_{r\,S\text{–}S}$) due to flow from the one step to the next. Figure 11 shows the prototype chute dimensions.

EVALUATION AND DISCUSSION OF RESULTS

Flow profiles on the stepped chute

Model Setup 1 – Horizontal steps with chute sidewall intact

The flow profiles were recorded for all test runs but the profiles for the maximum model overflow depth (y_{over} = 20 mm) will be used for illustrative purposes. Figure 12 presents a

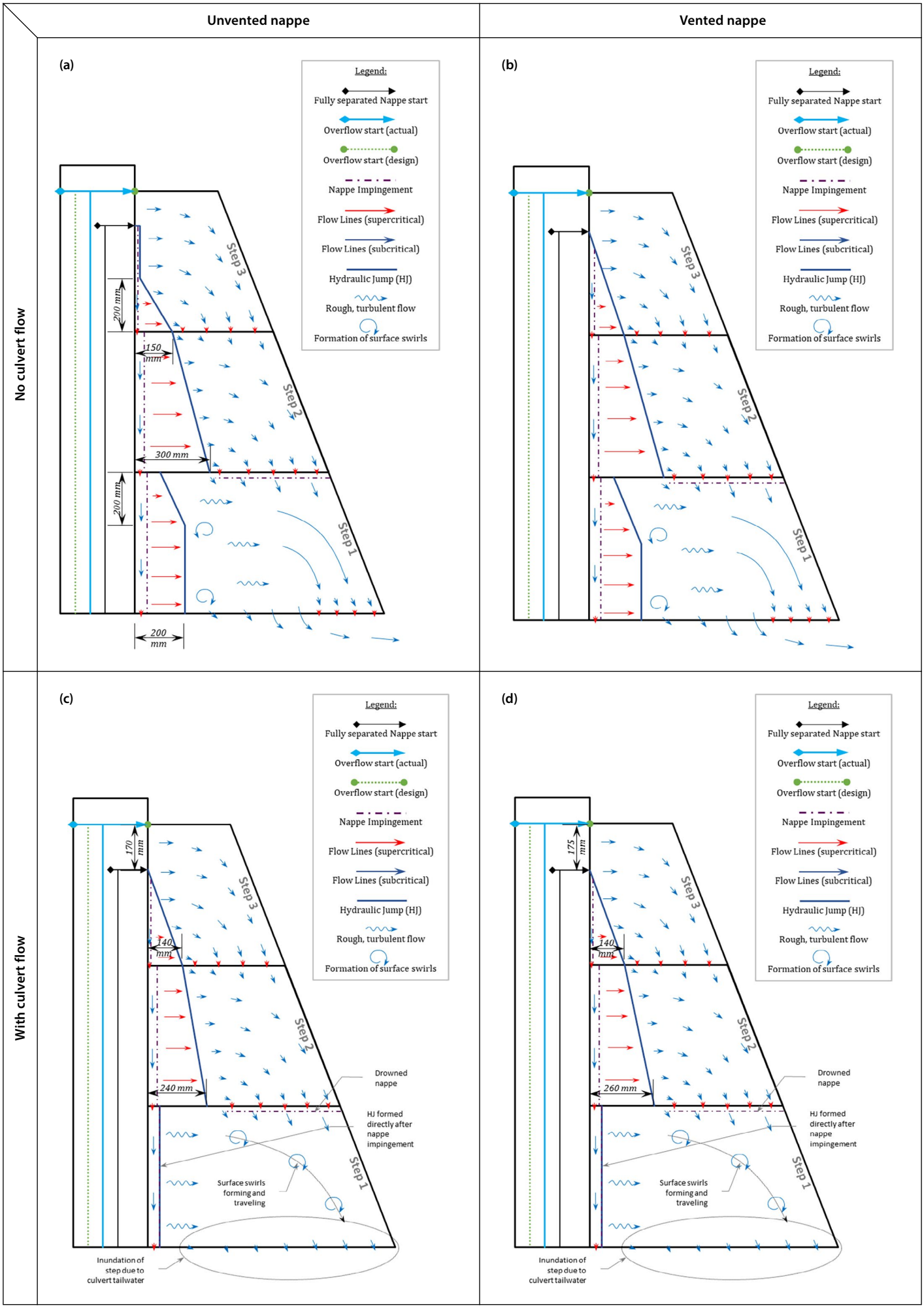

Figure 12 Hydraulic model flow profiles with chute sidewall intact with y_{over} = 20 mm

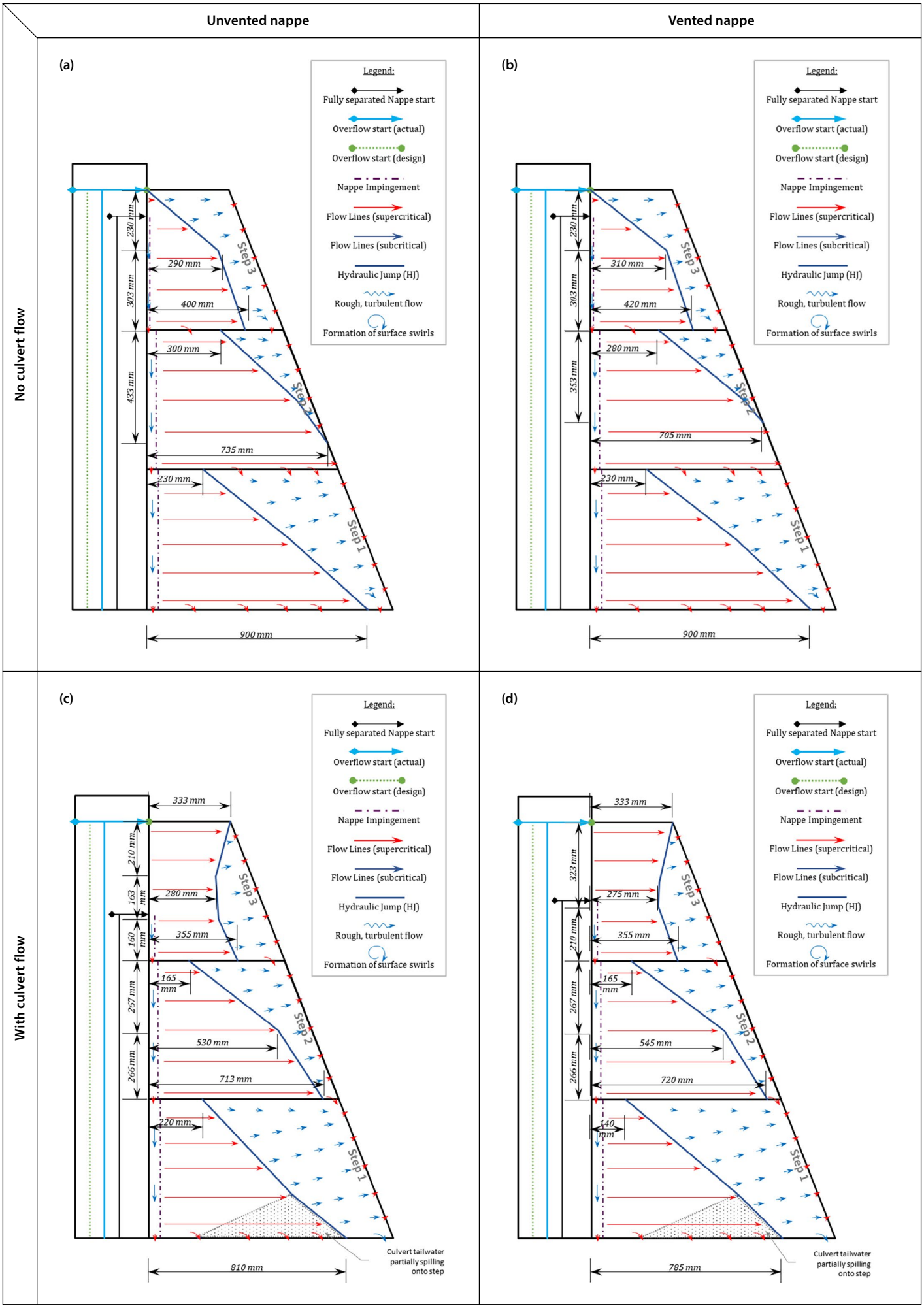

Figure 13 Hydraulic model flow profiles without chute sidewall with y_{over} = 20 mm

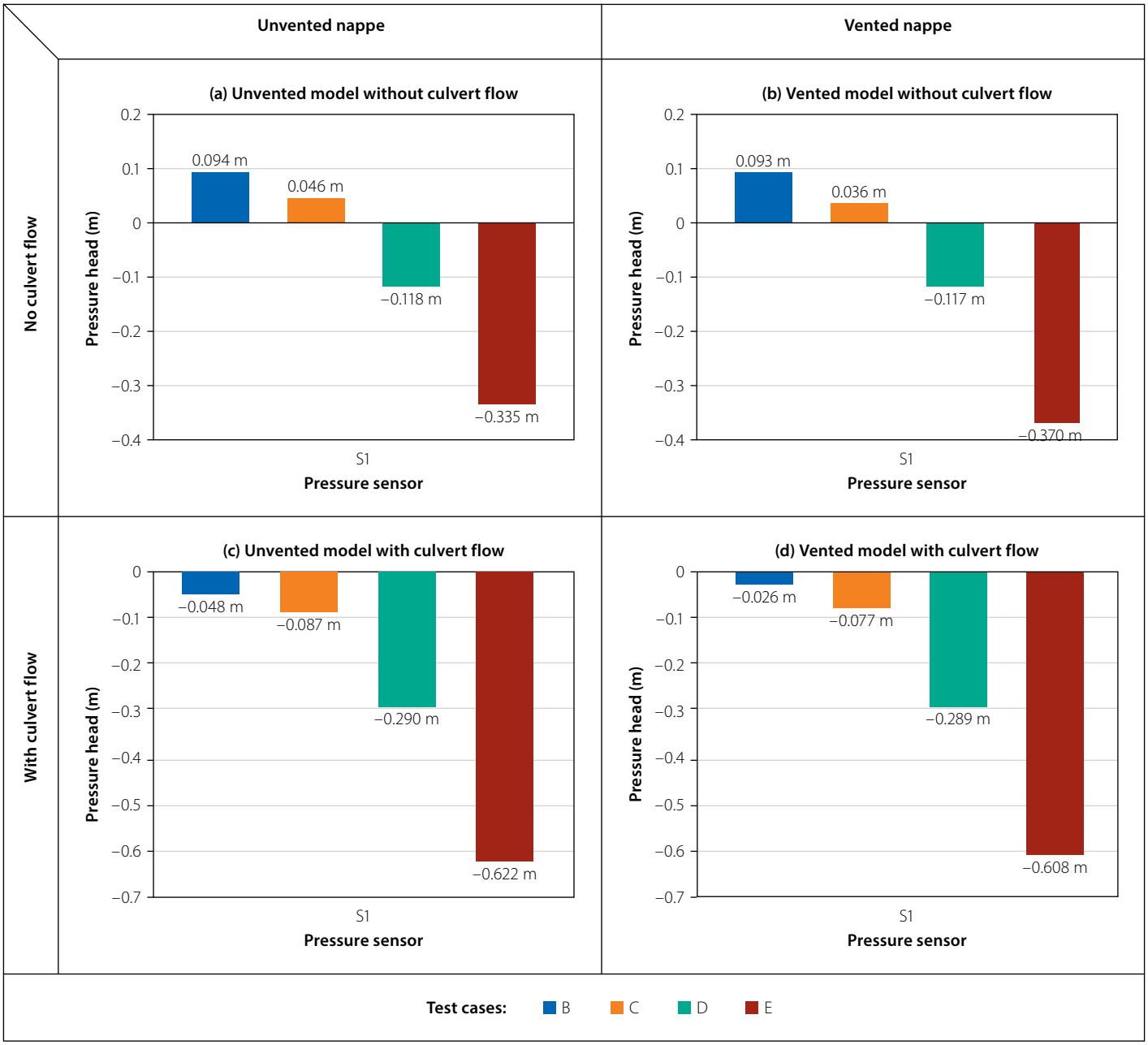

Figure 14 Prototype nappe cavity pressures

visual representation of the flow profiles for both the unvented and vented models, considering scenarios with and without culvert flow.

Significant similarities between the vented and unvented model were evident for both scenarios, whether with or without culvert flow. However, one notable difference was observed in the position of the hydraulic jump formation on step 3 for the flow profiles without culvert flow for the unvented and vented nappe tests, as depicted in Figures 12(a) and (b). The hydraulic jump positions remained the same for the remaining steps. In contrast, there were no discernible distinctions in the flow profiles between the unvented (Figure 12(c)) and vented (Figure 12(d)) configurations when culvert flow was present. Notably, the inundation of step 1 by the culvert tailwater also resulted in the formation of a partial hydraulic jump after the nappe's impingement from the approach road.

Drowned nappes were observed over the brink of steps 3 and 2 for flow in the direction of the chute. The concentration of flow was therefore insufficient to induce separation between the step face and the nappe, leading to the formation of a clinging nappe.

Model Setup 2 – Horizontal steps without chute sidewall

Figure 13 provides a visual representation of the flow profiles, depicting the unvented and vented model scenarios with and without culvert flow. Similarities were observed between the unvented and vented configurations for both culvert flow conditions, with consistent hydraulic jump positions maintained on all three steps for both the unvented and vented model configurations. A slight deviation was identified in the hydraulic jump position on step 1, shifting slightly to the left. This shift was attributed to the spillover of the culvert tailwater onto the bottom step, causing the formation of a standing wave.

Nappe formation occurred solely for flow from the approach road onto the chute steps, with no nappes forming from one chute step to the next. This observation was a consequence of the supercritical flow after the nappe impingement from the approach road, covering the majority of the step length before gradually transitioning into a weak hydraulic jump.

The position of the hydraulic jump varied for the two model configurations (chute sidewall intact, Figure 12, compared to no sidewall, Figure 13). In the first model

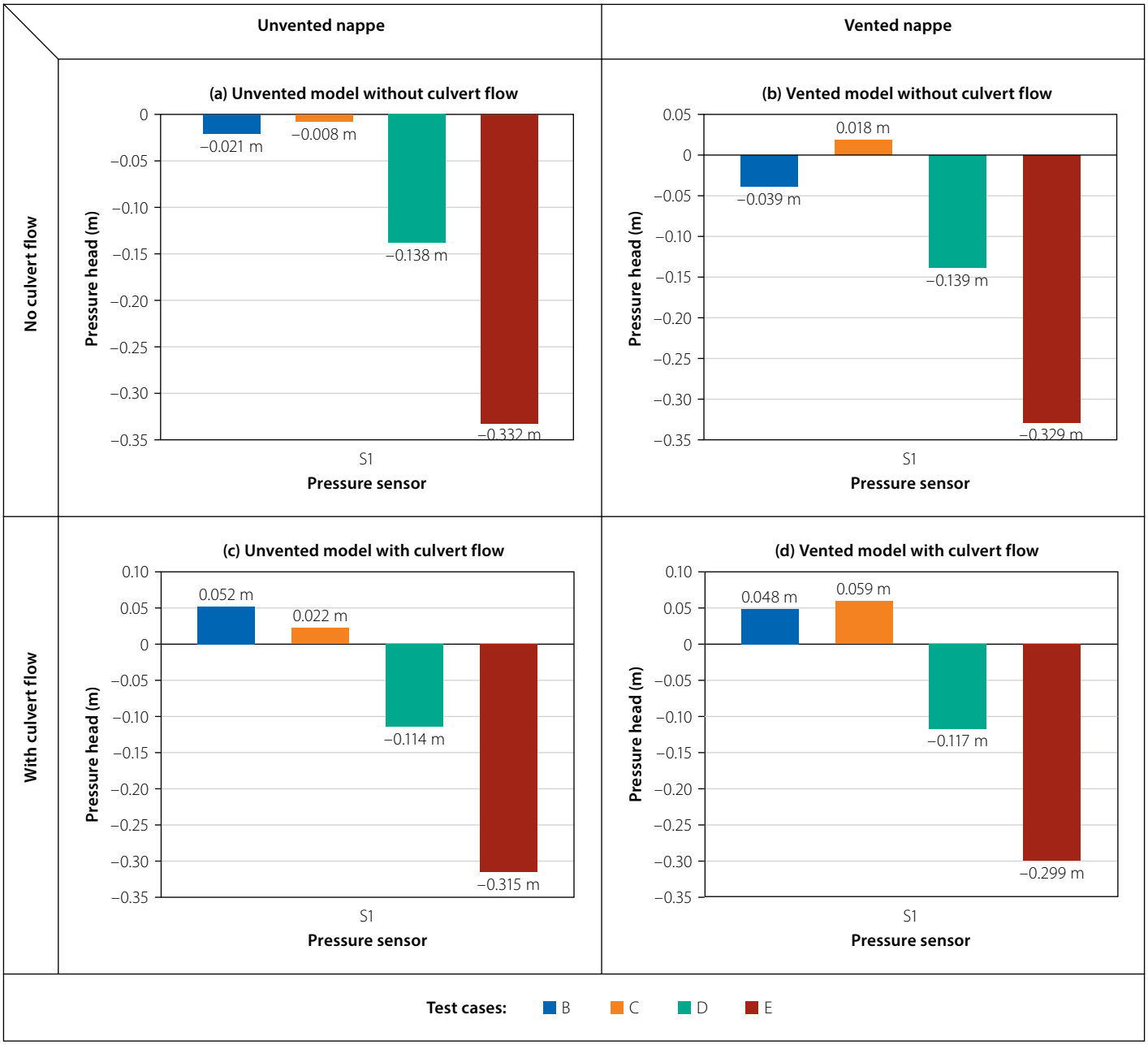

Figure 15 Prototype nappe cavity pressures

configuration (sidewall intact, Figure 12), the hydraulic jump formed in close proximity to the nappe impingement, while in the second model configuration (no sidewall, Figure 13) the hydraulic jump was situated further away from the nappe. This divergence was attributed to the accumulation of flow along the chute steps in the first model configuration, whereas the second model configuration did not experience the same flow accumulation phenomenon.

Nappe cavity pressures

The pressure readings obtained from transmitter S1 (location indicated on Figure 8) were used to describe the nappe cavity pressures, as the transmitter's position allowed for data collection during lower road overflow depths, given its close proximity to the culvert.

Model Setup 1 – Horizontal steps with chute sidewall intact

The pressure results for overflow depths of 180 mm to 300 mm confirmed the presence of negative nappe cavity pressures, as seen in Figure 14 (page 23). A discernible pattern emerged, revealing a gradual increase in negative pressure as the overflow depth increased. The nappe cavity pressures for the 60 mm and 120 mm overflow depths were due to the nappe forming from the approach road onto the chute steps not covering the S1 pressure sensor, or it did not form a fully separated nappe. The increase in negative nappe cavity pressure was caused by the increase in discharge resulting in a higher rate of air removal from the nappe cavity.

The average nappe cavity pressure, originating from the approach road, was 0.35 m below atmosphere for both unvented and vented nappe tests without culvert flow. In contrast, tests involving culvert flow for both unvented and vented nappes recorded an average nappe cavity pressure of 0.62 m. Minimal differences were noted in the pressure results between unvented and vented model configurations. The observed discrepancy in pressure between the tests with and without culvert flow seemed to be a result of the tailwater levels and the resultant nappe drop height. Tests without culvert flow exhibited significantly lower tailwater levels, allowing for the nappe to deform more easily, thereby limiting the pressure drop. Conversely, tests with culvert flow featured higher tailwater levels, resulting in a shorter nappe drop height that was less prone to deformation to easily accommodate the pressure drop.

The onset of cavitation is normally associated with the vapour pressure of a liquid, but due to dissolved gasses and small particles in suspension, cavitation damage may occur at higher pressures (Chadwick *et al* 2013). According to Chadwick *et al* (2013), pressures should not be allowed to fall below 3 m absolute (7 m below atmosphere). The maximum recorded pressure for sensor S1 was 0.687 m (Figure 14(c) – unvented model but with culvert flow) which falls well within this margin, and damage due to cavitation may therefore be disregarded.

Model Setup 2 – Horizontal steps without chute sidewall

The pressure reading results for Model Setup 2, depicted in Figure 15, confirmed the presence of sub-atmospheric pressure behind the fully separated nappe forming from the approach road onto the chute steps. A gradual increase in sub-atmospheric pressure with the increase in overflow depth was noted, aligning with the observations from the first model setup. However, the results for overflow depths of 120 mm and 180 mm (test cases B and C, respectively) introduced an element of ambiguity. Notably, the pressure recorded for the 180 mm overflow depth (test case B) was lower than the pressure for overflow depth of 240 mm (test case C) for most of the test for the second model configurations. While the exact cause remains uncertain, it is plausible that water ingress into the pressure probe during the test run may have contributed to irregular readings.

The maximum pressures generated by the nappe from the approach road onto the chute steps exhibited consistent magnitude for all four test cases (unvented, vented, without culvert flow and with culvert flow). The average pressures behind the nappe was 0.33 m below atmosphere for the tests without culvert flow (Figures 15(a) and (b)), and 0.31 m below atmosphere for tests with culvert flow (Figure 15(c) and (d)). Interestingly, the presence of culvert tailwater had no discernible impact on the nappe cavity pressures, mirroring the findings from Model Setup 1 where the chute wall remained intact. The tailwater did not reduce the nappe drop length, which allowed for nappe deformation, yielding comparable magnitudes of nappe cavity pressures. Importantly, these pressures were well within the cavitation threshold of 7 m below atmospheric pressure, thereby eliminating the possibility of cavitation damage.

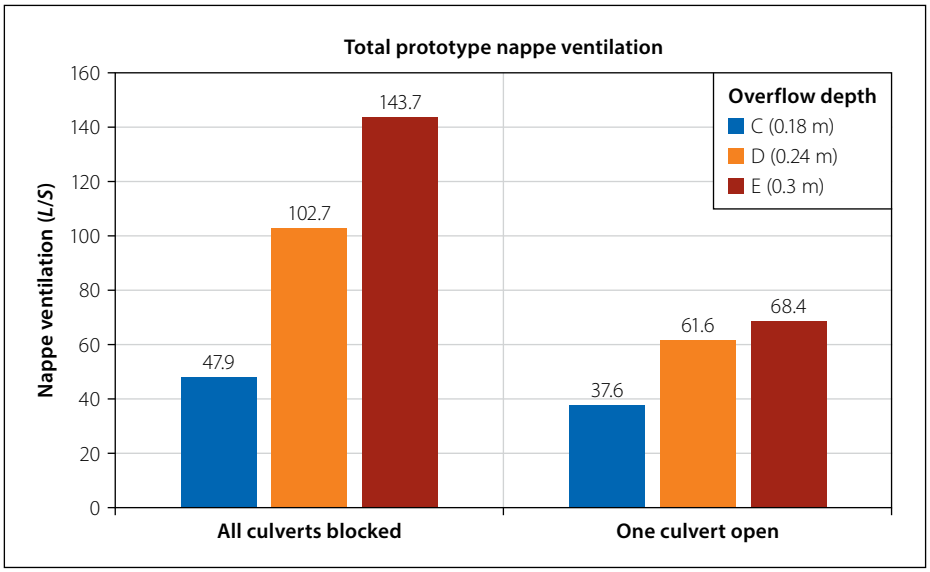

Figure 16 Total prototype nappe ventilation airflows – model with chute sidewall

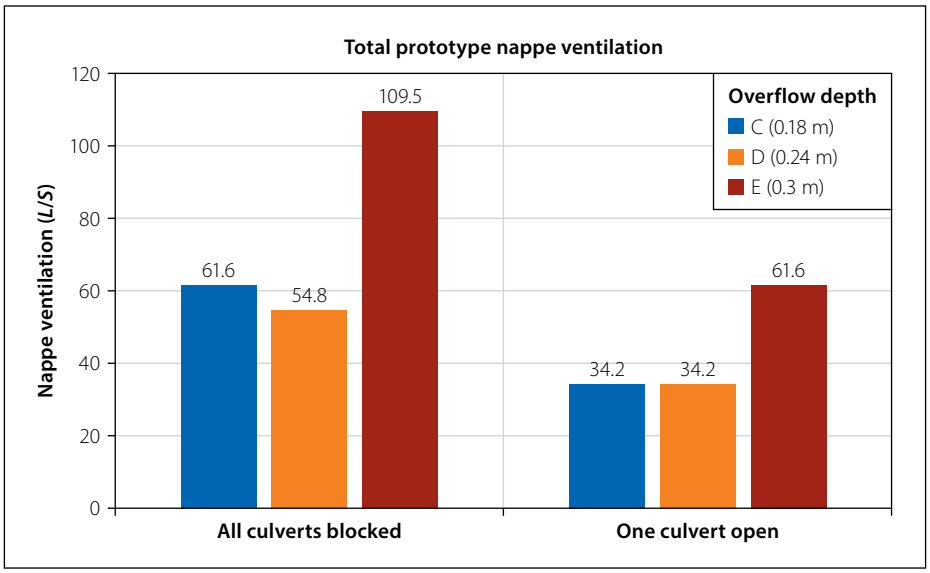

Figure 17 Total prototype nappe ventilation airflows – model without chute wall

Nappe cavity ventilation

Model Setup 1 – Horizontal steps with chute sidewall intact

Air vents V1 and V2 (location indicated in Figure 8) were added to steps 1 and 2, respectively, to ascertain the nappe airflow requirement from the approach road onto the stepped chute steps. The resulting airflow was converted into equivalent prototype values and are illustrated in Figure 16.

The nappe ventilation results revealed a proportional increase in airflow as the approach road overflow depth and corresponding discharge increased. This augmentation in airflow corresponded to an increased pressure differential between the atmospheric conditions and the sub-atmospheric nappe cavity.

Model Setup 2 – Horizontal steps without chute sidewall

The prototype equivalent nappe ventilation airflow values for the second model setup (horizontal steps without chute sidewall) are illustrated in Figure 17.

The results indicated an increase in airflow corresponding to increase in the approach road discharge, except in both D test cases (prototype approach road overflow depth of 0.24 m). While a similar trend was anticipated as observed in Model Setup 1, the minimal quantity of airflow, and the subsequently low measured air velocities approached the anemometer's minimum measurable limit. This discrepancy between the airflows in the first and second model setups was attributed to the anemometer's near-limit condition. The nappe ventilation from the approach road onto the steps was considerably lower than the initial estimated

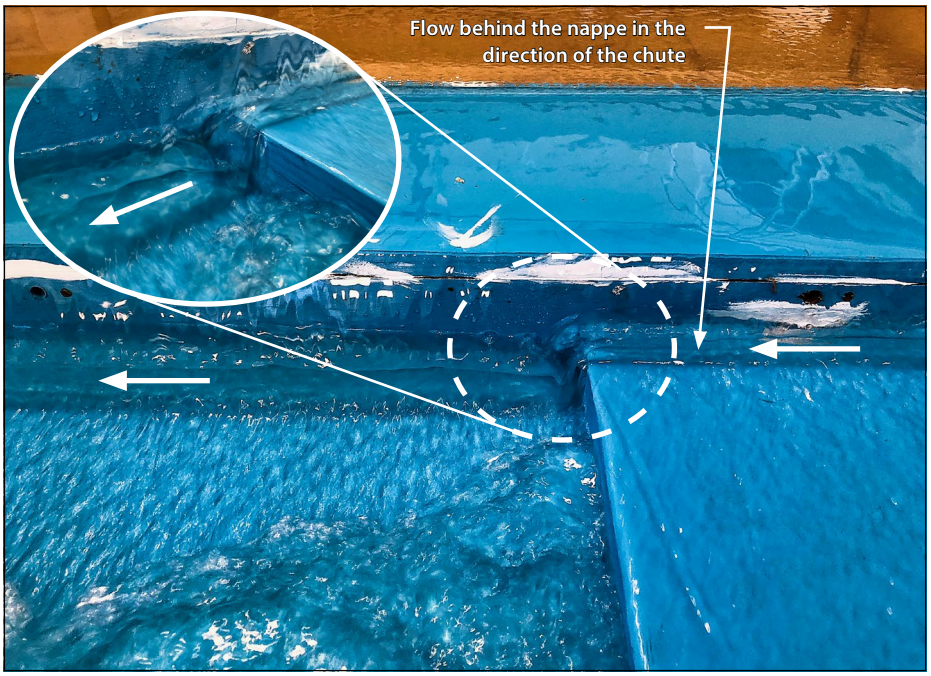

Figure 18 Lateral flow down the chute steps behind the nappe

prototype airflow of 0.225 m³/s for both model configurations.

Other notable observations for Model Setups 1 and 2

Lateral flow within the nappe cavity

Flow behind the fully developed nappe, forming from the approach road and directed towards the main channel, was evident during tests and is shown in Figure 18. This resulted in a reduction of flow continuing to the hydraulic jump on each step, but this reduction could not be measured.

Hydraulic ventilation of the nappe cavity

Test instances with culvert flow revealed that the intersection line of the nappe and culvert outflow induced turbulence, resulting in the formation of breakaway air bubbles. These air bubbles were transported along the intersection line, acting as a hydraulic ventilation for the rear of the nappe. The breakaway air bubbles appeared to serve as an alternative source of nappe ventilation, contributing to the reduction in nappe airflow in tests with culvert flow compared to those tests without culvert flow.

Figure 19 illustrates the difference between the nappes downstream of the culvert where Figure 19(a) has no culvert flow and Figure 19(b) has culvert flow. Figure 19(a) shows no air bubbles forming downstream of the culvert, whereas Figure 19(b) shows the intersection line generating a string of air bubbles transported in the direction of the red arrows. Some of the air bubbles were conveyed either to the nappe cavity, while the remainder travelled downstream.

Performance of model variations

Three model variations were introduced, namely backward sloping steps, steps with pooled cascades and steps with baffle blocks, as illustrated in Figures 7(c), 7(d) and 7(e), respectively. The downstream energy depths for these three model variations were evaluated in comparison to the model featuring the horizontal steps (Figure 7(a) – Model Setup 1). The objective was to ascertain which model variation exhibited the most effective rate of energy dissipation. The percentage difference in the downstream energy depth of each of the three model variations compared to the horizontal steps model configuration as illustrated in Figure 20.

The similarity in the energy head percentage difference for the low overflow depth (0.06 m) for the model variations and Model Setup 1 suggests that fluid tension and viscosity most likely influenced the results, given the low overflow depth. Conversely, larger overflow depths (>0.06 m) showed that the model variations exhibited higher downstream energy depths, signifying less energy dissipation. Further examination of the flow field on the steps for the three model variations revealed locally submerged flow conditions on each step, contributing to the reduced energy dissipation.

In summary, the model with horizontal steps (Model Setup 1) proved to be more effective in energy dissipation. Additionally, the simpler layout of the horizontal steps renders this configuration more favourable from both a construction and a maintenance perspective.

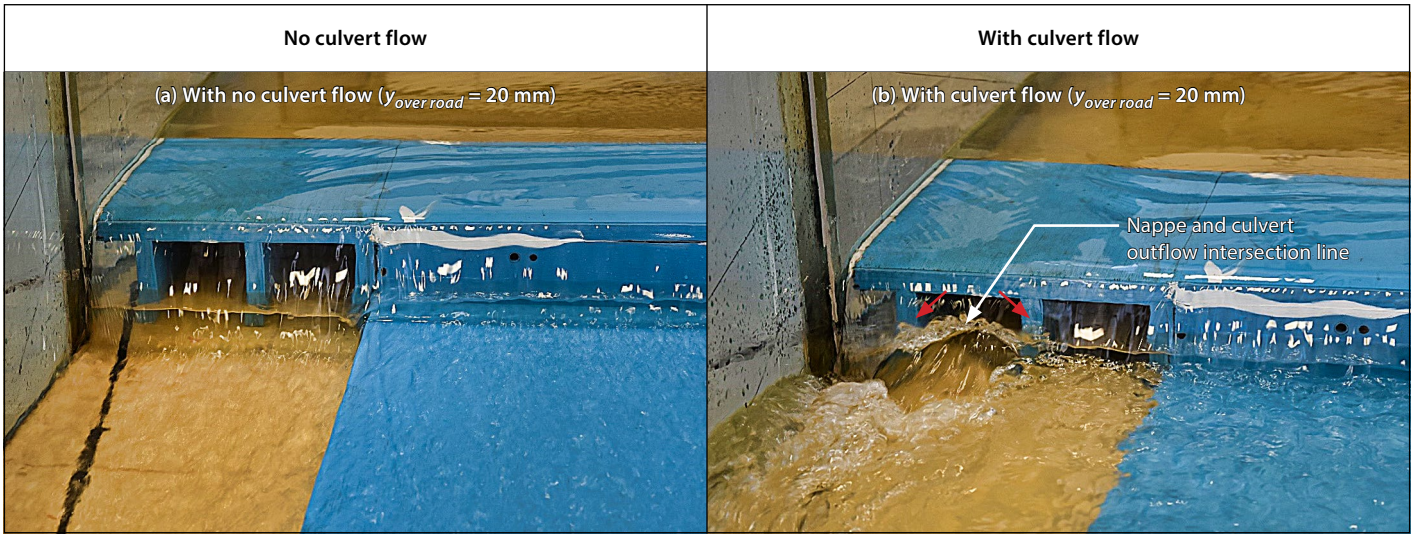

Figure 19 Nappe impingement

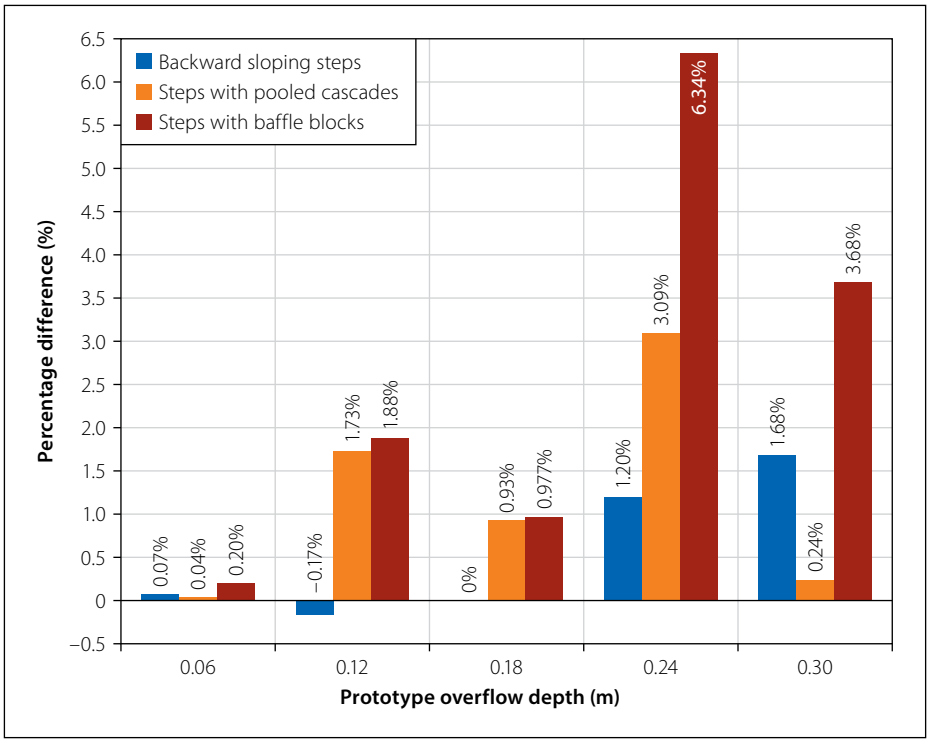

Figure 20 Energy head difference compared to horizontal steps model configuration

REGRESSION ANALYSIS

A regression analysis was performed on the experimental results aimed to establish design formulae for the stepped chute geometry. However, the step height, step width, and the number of steps were observed to be dependent on the geometry of the low-level river crossing structure and the overflow depth. Consequently, the design procedure mentioned earlier in this article and described in detail by Cloete (2019) is recommended as the preferred method for determining the chute dimensions.

A non-dimensional multi-linear regression analysis was performed which revealed that the ratio of the step length to the approach road overflow depth (ϕ_0) is a function of two dimensionless independent variables (ϕ_1 and ϕ_2) as indicated in Equation 10:

$$\phi_0 = f(\phi_1, \phi_2) \tag{10}$$

Where:

$$\phi_0 = \frac{L_{step\ (ns)}}{y_{over\ road\ (ns)}}$$

$$\phi_1 = \frac{h_{R-S\ (ns)}}{y_{over\ road\ (ns)}}$$

$$\phi_2 = \frac{Q_{S-S\ (ns+1)}}{Q_{R-S\ (ns)}}$$

with ns the number of the steps in question, provided that the steps are numbered from the bottom to the top step.

Three multi-linear regression models were considered (linear, log-transformed and linear-log regression models) of which the linear regression model exhibited the best fit, indicated by the highest coefficient of determination. The explicit form of the equation to predict the length of a chute step (Equation 11), based on the coefficients derived from the linear regression model, is expressed as follows:

$$L_{step\ (ns)} = y_{over\ road\ (ns)} \times \left[12.744 + 10.05 \cdot \frac{h_{R-S\ (ns)}}{y_{over\ road\ (ns)}} - 7.515 \cdot \frac{Q_{S-S\ (ns+1)}}{Q_{R-S\ (ns)}}\right] \tag{11}$$

The regression formula should be applied inside the prototype ranges in which the formula was developed ($h_{R-S} \leq 1.275$ m, $y_{over\ road\ (ns)} \leq 0.3$ m, and low-level river crossing deck crossfall = 0%).

It is advisable to verify that the conjugate flow depth, after the hydraulic jumps are formed in the direction of the chute, remains less than the step height (h_{S-S}) after determining the chute length using Equation 11. If this condition is not met, reducing the number of steps (ns) to increase the step height is recommended.

The data set used in the regression analysis was limited to a road crossfall of 0%. To enhance the analysis, incorporating additional data for crossfalls exceeding 0% is recommended.

CONCLUSIONS

During high river flow events, the potential for downstream erosion of the river embankments due to flow overtopping a low-level river crossing is a critical concern. Implementing a stepped chute downstream of the approach roads is considered an effective strategy for dissipating excess energy, thereby mitigating the scour potential of the overflow water.

Model Setup 1, featuring horizontal steps with the chute wall intact, performed the best in terms of energy dissipation. Sub-atmospheric nappe cavity pressures (ranging from 0.335 m to 0.622 m) were observed during maximum road overflow, for tests with and without nappe ventilation, as well as tests with and without culvert flow. While pressures varied slightly under different culvert flow conditions, they remained within the same order of magnitude and well below the cavitation threshold.

The results from the physical model were used to develop a non-dimensional multi-linear regression formula to predict the step length in the direction of the flow, offering practical applications for future low-level river crossing designs. The use of a stepped chute downstream of low-level river crossings presents a promising solution for mitigating the erosive potential of high-flow events.

CHUTE DESIGN RECOMMENDATIONS

The following aspects can be used as design and application guidelines for a stepped chute:

1. Overflow depth recommendations: Adhere to recommended overflow depth limits of 100 mm for supercritical flow and 150 mm for subcritical flow during annual floods, as suggested by Pienaar and Kruger (2013).
2. Road design guidelines: Follow Pienaar and Kruger (2013) specifications, ensuring an approach road slope of less than 10% for unpaved roads and 12% for paved roads. Single-lane crossings should have a width of 4 m, and two-lane crossings should have a width of 7.5 m.
3. Flow regime considerations: Avoid the transition flow zone when designing stepped chutes. This will maintain the nappe flow regime for optimal performance.
4. Artificial ventilation considerations: Artificial ventilation of the nappe cavity was found not to enhance energy

dissipation. However, ventilation could mitigate possible cavitation problems on the steps.

5. Chute dimension criteria: Adhere to three key conditions for determining the stepped chute dimensions:
   a. Ensure that the conjugate depth of the hydraulic jump between steps does not exceed the step height to prevent inundation of the previous step.
   b. Keep the combined length of the nappe drop and hydraulic jump roller less than the step length.
   c. Maintain nappe flow conditions in the direction of the stepped chute.
6. Culvert tailwater analysis: Conduct a detailed analysis of the culvert tailwater conditions. Further research is recommended to explore the mitigation measures in averting inundation of the lowermost step, such as adjusting the step heights to increase the bottom step height or reducing the step widths to create distance between the last step and the nearest culvert opening.

NOTATIONS

Symbol	Description	Units
C_b	Coefficient expressing the effect of width contraction in the flow	dimensionless
C_h	Coefficient of contraction in the vertical plane	dimensionless
D	Height of the culvert opening	m
Fr_1	Froude number at section 1	dimensionless
g	Gravitational acceleration constant taken as 9.81 m/s^2	m/s^2
H_1	Energy head at section 1	m
$h_{R–S}$	Nappe drop height from the LLRC approach road onto the chute step	m
$h_{S–S}$	Chute step height	m
L_d	Horizontal length of a nappe drop, measured from the face of the drop to the impingement point	m
$L_{d\,R–S}$	Horizontal length of the nappe drop formed from the LLRC approach road onto the chute step	m
$L_{d\,S–S}$	Horizontal length of the nappe drop formed from one chute step onto the next chute step	m
L_r	Length of the hydraulic jump roller taken to the point where the flow velocity at the top reverses and the jet continues (Chaudry 2008)	m
$L_{r\,R–S}$	Horizontal length of the hydraulic jump, formed from the approach road, on the chute step	m
$L_{r\,S–S}$	Horizontal length of the hydraulic jump formed from one chute step onto the next chute step	m
$L_{Step\ (ns)}$	Length of chute step number *ns*	m
ns	The number of the chute step in question	dimensionless
n_{steps}	Number of chute steps	dimensionless
Q_{air}	Air-flow rate required to ventilate the nappe cavity	m^3/s
$Q_{R–S\ (ns)}$	Flow from the approach road onto chute step number *ns*	m^3/s
$Q_{S–S\ (ns)}$	Flow from the previous chute step (*ns*+1) onto step number *ns*	m^3/s
r^2	Coefficient of determination	dimensionless
$w_{culvert}$	Width of the culvert opening	m
y_n	Flow depth at section number *n*	m
y_b	Overflow depth at the brink of a step	m
y_c	Critical flow depth	m
$y_{over\ road}$	Flow depth on top of the LLRC deck	m
y_p	Pool depth beneath the nappe	m
y_{top}	Flow depth from the step above the receiving step	m
l	Stepped chute spillway step length	m

ACKNOWLEDGEMENTS

This research was conducted in the Civil Engineering Department at Stellenbosch University, South Africa. The opinions expressed, and conclusions arrived at, are those of the authors.

REFERENCES

Bos, M G 1989. *Discharge Measurement Structures,* 3rd ed. The Hague, Netherlands: International Institute for Land Reclamation and Improvement.

Chadwick, A, Morfett, J & Borthwick, M 2013. *Hydraulics in Civil and Environmental Engineering,* 5th ed. Boca Raton, FL: Taylor & Francis.

Chanson, H 1994. Hydraulics of nappe flow regime above stepped chutes and spillways. *Australian Civil Engineer Transactions*, CE36(1): 69–76.

Chanson, H 2001. *Experimental investigations of air entrainment in transition and skimming flows down a stepped chute.* Research Report No CE 158. Australia: University of Queensland.

Chaudry, M H 2008. *Open-Channel Flow,* 2nd ed. New York: Springer Science & Business Media.

Cloete, P 2019. *Protection of river embankments downstream of low-level river crossings using stepped chute energy dissipation structures.* University of Stellenbosch.

Hager, W H, Bremen, R, Bremen, N & Kawagoshi, N 1990. Classical hydraulic jump length: Length of roller. *Journal of Hydraulic Research,* 28(5): 591–608.

Heller, V 2011. Scale effects in physical hydraulic engineering models. *Journal of Hydraulic Research,* 49(3): 293–306. doi: 10.1080/00221686.2011.578914.

Henderson, F M 1966. *Open Channel Flow.* New York: Macmillan.

Johannessen, B 2008. *Building Rural Roads.* Bangkok: International Labour Organization (ILO).

Khatsuria, R M 2005. *Hydraulics of Spillways and Energy Dissipators.* New York: Marcell Dekker.

Peyras, L, Royet, P & Degoutte, G 1992. Flow and energy dissipation over stepped gabion weirs. *Journal of Hydraulic Engineering, ASCE,* 118(5): 707–717.

Pienaar, P A & Kruger, E J 2013. *Road Drainage Manual: Chapter 6: Low-level River Crossings,* 6th ed. Pretoria: South African National Roads Agency SOC Ltd (SANRAL).

Rooseboom, A & Van Vuuren, S J 2013. *Road Drainage Manual. Chapter 7: Lesser Culverts (and Stormwater Conduits),* 6th ed. Pretoria: South African National Roads Agency SOC Ltd (SANRAL).

Vos, A 2011. *Unsteady flow conditions at dam bottom outlet works due to air entrainment during gate closure: Berg River Dam Model.* Report. University of Stellenbosch.